Received: 13 September 2019 | Revised: 22 July 2020 | Accepted: 9 August 2020

DOI: 10.1002/col.22563

RESEARCH ARTICLE

WILEY

An efficient nonlinear polynomial color characterization method based on interrelations of color spaces

Jing Ji[1,2] | **Suping Fang**[1] | **Zhengyuan Shi**[3] | **Qing Xia**[3] | **Yibao Li**[3]

[1]Xi'an Jiaotong University, State Key Laboratory of Manufacturing Systems Engineering, Xi'an, China

[2]Xi'an Jiaotong University Museum, Xi'an Jiaotong University, Xi'an, China

[3]School of Mathematics and Statistics, Xi'an Jiaotong University, Xi'an, China

Correspondence
Suping Fang, Xi'an Jiaotong University, State Key Laboratory of Manufacturing Systems Engineering, Xi'an 710049, China.
Email: spfang@mail.xjtu.edu.cn

Funding information
China Postdoctoral Science Foundation, Grant/Award Number: 2018M640968; Fundamental Research Funds for the Central Universities, Grant/Award Number: XTR042019005; National Natural Science Foundation of China, Grant/Award Number: 11601416

Abstract

A well-known color characterization method is to take an image of a color chart and then to find the mapping matrix from the digital RGBs to the corresponding known CIEXYZs. However, the prediction errors are generally large in CIELAB color space because of the nonlinear transformation from CIEXYZs to CIELABs. In this article, we propose an efficient and simple nonlinear method for the color characterization of input devices. The approach for deriving a colorimetric mapping between digital RGB signals and CIELAB tristimulus values uses the polynomial modeling by considering the interrelations among the standard CIE color spaces. Furthermore, to improve the accuracy of solution, we take the polynomial root terms extension. Our algorithm is simple to implement because only a least-squares mapping should be solved. Various computational results are given to demonstrate the efficiency and capability of the proposed method.

KEYWORDS

color characterization, color correction, nonlinear transformation, polynomial regression

1 | INTRODUCTION

A digital camera is an effective device to record color information with pixel accuracy. It is widely applied in color reproduction without contacting the objects, especially in cultural relics high-fidelity digital reproduction.[1-3] However, the images captured by cameras rely on devices and light source. RGB responses of the same image are different by different filming conditions, which severely limit the application of cameras in color reproduction. Therefore, RGB information captured by the camera needs to be converted to a standard color space independent of interfering factors. This process is called color characterization.[4]

Typical color characterization methods include three-dimensional look-up table method with interpolation and extrapolation,[5,6] polynomial modeling method,[7] and neural network.[8] For the look-up table method, a large training set is necessary as proposed in Reference 9. The method of neural network can produce good effects in nonlinear mapping, but its processing speed is low and a lot of samples are needed.[10,11] Comparing with the previous methods, the polynomial modeling method is more practical and efficient because it only needs a reference target with a certain number of color samples. Kang[7] transformed digital RGB values preprocessed by gray balance to CIEXYZ color space using polynomial regression. The author summarized that the fitting accuracy of training data is improved and the accuracy of testing data may be worse as the order of polynomials increasing. Hong et al[12,13] used different polynomials and 8-bit and 12-bit digital RGB data to test the accuracy of color characterization. They also

compared the color characterization performance between the high-end and low-end digital cameras and pointed out the range of possibilities for improving the accuracy of color characterization. Hardeberg[14,15] introduced a preprocess of polynomial regression in which a cubic root of RGB values was used. Andersen et al[16] proposed a method called Hue Plane Preserving Color Correction (HPPCC) which matches digital RGBs to CIEXYZs in each hue slice of color space with different polynomial transformations. Huang et al[17] improved the polynomial modeling by replacing the inherent camera RGB values with normalized luminance. Finlayson et al[18] proposed the white preserving color correction which is well-behaved when the training set is incomplete. However, this method may result in a higher mean error than conventional color correction while exactly matching the white patch. After that, they proposed root-polynomial color correction related to the idea of fractional polynomials.[19] In the above research, the polynomial regression was used to transform digital RGB values to CIEXYZ values. However, as the CIEXYZ space is an nonuniform color space, the minimized error obtained by regression algorithm in the CIEXYZ space is poorly correlated to visual color differences, thus leading to unsatisfactory results.

In this article, we set a polynomial regression model using CIELAB space as the destination color space, because Euclidean distance in this space can evaluate perceptual color differences reasonably well. The main contribution of this article is to improve the accuracy of color characterization through the following two aspects: First, comparing with the previous related studies,[14,20] our proposed method considers the interrelation among the standard CIE color spaces and presents a complete theoretical derivation form the device-dependent color space to the standard CIELAB space. Second, the polynomial root terms extension is constructed in our proposed method to further improve the transformation accuracy. To avoid misunderstanding, we have to point that our method is not exposure invariant (as mentioned in Reference 19) due to the nonlinear transformation from digital RGB values to CIELAB values. Various tests have been performed to verify the performance of the proposed method at the same exposure level.

The rest of this article is organized as follows: The background of polynomial approach on color characterization is presented in Section 2. Our method is drawn in Section 3. The experiments are presented in Section 4. The conclusion is given in Section 5.

2 | PROBLEM FORMULATION AND RELATED WORKS

2.1 | Polynomial color characterization

A color chart with a set of n color samples is scanned. For each color sample, the corresponding tristimulus value is known and defined as a three-dimensional vector $\boldsymbol{q}$ ($\boldsymbol{q} \in \mathbb{R}^{3\times 1}$) and the device three-dimensional digital response is defined as $\boldsymbol{\rho}$ ($\boldsymbol{\rho} \in \mathbb{R}^{3\times 1}$). A simple linear color characterization transformation can be written as follows:

$$\boldsymbol{M}\cdot\boldsymbol{\rho} = \boldsymbol{q}. \tag{1}$$

Vector $\boldsymbol{\rho}$ can be extended to m dimensions by increasing basis function in polynomial regression. For the first, second, third, fourth, and fifth order polynomial expansions, vector $\boldsymbol{\rho}$ is depicted by $\boldsymbol{\rho}_k^n$ ($k = 1,2,3,4,5$ and n is the number of terms) as

$$\begin{cases}
\boldsymbol{\rho}_1^4(r,g,b) = (1,r,g,b)^T \\
\boldsymbol{\rho}_2^{10}(r,g,b) = (1,r,g,b,r^2,g^2,b^2,rg,rb,gb)^T \\
\boldsymbol{\rho}_3^{20}(r,g,b) = \left(1,r,g,b,r^2,g^2,b^2,rg,rb,gb,r^3,g^3,b^3,rg^2,r^2g,gb^2,g^2b,rb^2,r^2b,rgb\right)^T \\
\boldsymbol{\rho}_4^{35}(r,g,b) = (1,r,g,b,r^2,g^2,b^2,rg,rb,gb,r^3,g^3,b^3,rg^2,r^2g,gb^2,g^2b,rb^2,r^2b,rgb,r^4, \\
\qquad g^4,b^4,gr^3,br^3,rg^3,bg^3,rb^3,gb^3,gbr^2,rbg^2,rgb^2,r^2g^2,r^2b^2,b^2g^2)T \\
\boldsymbol{\rho}_5^{56}(r,g,b) = (1,r,g,b,r^2,g^2,b^2,rg,rb,gb,r^3,g^3,b^3,rg^2,r^2g,gb^2,g^2b,rb^2,r^2b,rgb,r^4, \\
\qquad g^4,b^4,gr^3,br^3,rg^3,bg^3,rb^3,gb^3,gbr^2,rbg^2,rgb^2,r^2g^2,r^2b^2,b^2g^2,r^5,g^5,b^5, \\
\qquad gr^4,br^4,rg^4,bg^4,rb^4,gb^4,g^2r^3,b^2r^3,gbr^3,r^2g^3,b^2g^3,brg^3,g^2b^3,r^2b^3,grb^3, \\
\qquad gb^2r^2,bg^2r^2,rg^2b^2)T.
\end{cases}$$

We define $\boldsymbol{P}$ ($\boldsymbol{P} \in \mathbb{R}^{m \times n}$, $m \ll n$) as a $m \times n$ matrix of vector $\boldsymbol{\rho}$ and $\boldsymbol{Q}$ ($\boldsymbol{Q} \in \mathbb{R}^{3 \times n}$) as the corresponding matrix of vector $\boldsymbol{q}$. The mapping relationship between the camera response space and the corresponding tristimulus value space can be represented by

$$\boldsymbol{M} \cdot \boldsymbol{P} = \boldsymbol{Q}, \tag{2}$$

where $\boldsymbol{M}$ is the mapping matrix that depends on $\boldsymbol{P}$ and $\boldsymbol{Q}$. The key of color characterization is to find the optimal mapping matrix $\boldsymbol{M}$.

2.2 | Color space conversion formula

The CIE 1931 Standard RGB Colorimetric System (CIERGB), a basis in colorimetry, is a linear transformation of the CIE 1931 Standard XYZ Colorimetric System (CIEXYZ) as

$$\begin{bmatrix} X \\ Y \\ Z \end{bmatrix} = \boldsymbol{A} \cdot \begin{bmatrix} R \\ G \\ B \end{bmatrix}, \tag{3}$$

where $\boldsymbol{A}$ is

$$\boldsymbol{A} = \begin{bmatrix} 2.7689 & 1.7517 & 1.1302 \\ 1.0000 & 4.5907 & 0.0601 \\ 0.0000 & 0.0565 & 5.5943 \end{bmatrix}. \tag{4}$$

The CIELAB space is an uniform color space for practical applications, which is defined by the quantities L, a, and b. The relationship between CIELAB and CIEXYZ is defined as follows:

$$\begin{cases} L = 116 f\left(\dfrac{Y}{Y_n}\right) - 16 \\ a = 500\left[f\left(\dfrac{X}{X_n}\right) - f\left(\dfrac{Y}{Y_n}\right)\right], \\ b = 200\left[f\left(\dfrac{Y}{Y_n}\right) - f\left(\dfrac{Z}{Z_n}\right)\right] \end{cases} \tag{5}$$

where

$$f(a) = \begin{cases} a^{\frac{1}{3}} & \text{if } a \geq 0.008856 \\ 7.787a + \dfrac{16}{116} & \text{otherwise.} \end{cases} \tag{6}$$

It should be pointed that $f(a)$ can be simplified as $f(a) = a^{\frac{1}{3}}$, because $7.787a + 16/116 \approx a^{\frac{1}{3}}$, if $a < 0.008856$. X_n, Y_n, and Z_n denote the tristimulus values of nominally white stimulus. A widely used method comparing two colors denoted by $[L_1, a_1, b_1]$ and $[L_2, a_2, b_2]$ is to calculate the Euclidean distance in CIELAB space as

$$\Delta E_{\text{ab}} = \sqrt{(L_1 - L_2)^2 + (a_1 - a_2)^2 + (b_1 - b_2)^2}. \tag{7}$$

As the evaluation criteria proposed in Reference 21, if $\Delta E_{\text{ab}} \in [0\ 3]$, the quality of color characterization is very good. If $\Delta E_{\text{ab}} \in (3\ 6]$, its quality is good. If $\Delta E_{\text{ab}} \in (6\ 10]$, its quality is sufficient. Otherwise, its quality is insufficient.

2.3 | Classic color characterization models

The relationship between source color space and destination color space is presented in Figure 1A. Several

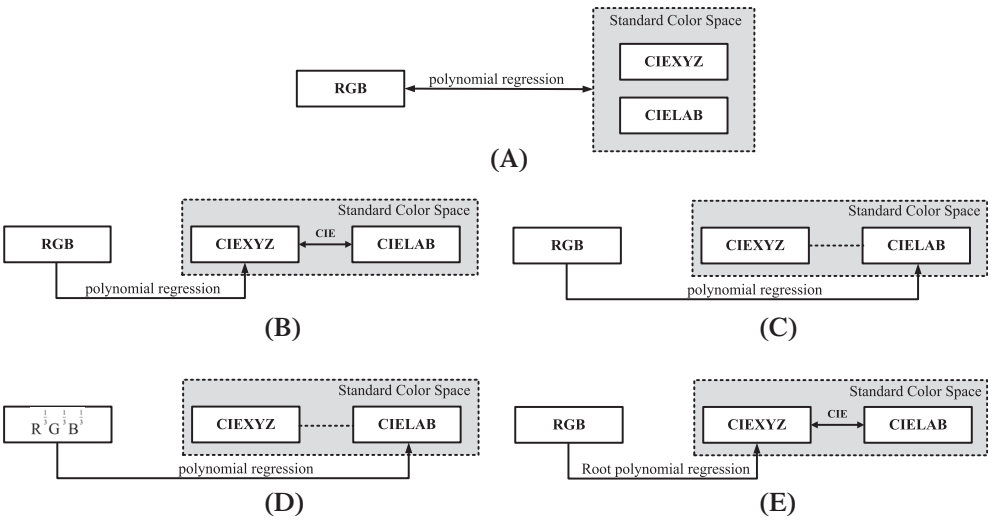

FIGURE 1 Classic color characterization models

classic color characterization models are available based on model-transformation methods and the destination color space.

Figure 1B shows the polynomial regression to CIEXYZ space.[12] The digital RGB values are transformed to CIEXYZ values by polynomial regression. And then CIELAB values can be derived from CIEXYZ values by a standardized formula which has been illustrated in Equation (5).

Figure 1C shows the polynomial regression to CIELAB space.[20] It is clear that the relationship between digital RGB values and CIELAB values is nonlinear. Therefore, *n*-order polynomial regression is used to model the transformation.

Figure 1D shows Hardeberg's method,[14] which applied a nonlinear correction to the digital RGB values before polynomial regression in the form of cubic squares. Here $\boldsymbol{\rho}_k^n(r,g,b)$ are replaced by $\boldsymbol{\rho}_k^n\left(r^{\frac{1}{3}},g^{\frac{1}{3}},b^{\frac{1}{3}}\right)$.

Finlayson's method[19] aims to find the root-polynomial expansions (RPCC) of all *k*-order polynomial as shown in Figure 1E. The root-polynomial expansions $\boldsymbol{\rho}_k^n(k=1,2,3,4)$ are given below:

$$\begin{cases} \boldsymbol{\rho}_1^3 = (r,g,b)^T \\ \boldsymbol{\rho}_2^6 = \left(r,g,b,\sqrt{rg},\sqrt{gb},\sqrt{rb}\right)^T \\ \boldsymbol{\rho}_3^{13} = \left(r,g,b,\sqrt{rg},\sqrt{gb},\sqrt{rb},\sqrt[3]{rg^2},\sqrt[3]{gb^2},\sqrt[3]{rb^2},\sqrt[3]{gr^2},\sqrt[3]{bg^2},\sqrt[3]{br^2},\sqrt[3]{rgb}\right)^T \\ \boldsymbol{\rho}_4^{22} = (r,g,b,\sqrt{rg},\sqrt{gb},\sqrt{rb},\sqrt[3]{rg^2},\sqrt[3]{gb^2},\sqrt[3]{rb^2},\sqrt[3]{gr^2},\sqrt[3]{bg^2},\sqrt[3]{br^2},\sqrt[3]{rgb} \\ \sqrt[4]{r^3g},\sqrt[4]{r^3b},\sqrt[4]{g^3r},\sqrt[4]{g^3b},\sqrt[4]{b^3r},\sqrt[4]{b^3g},\sqrt[4]{r^2gb},\sqrt[4]{g^2rb},\sqrt[4]{b^2rg})T \end{cases}$$

In this method, the root polynomial regression is applied to transform digital RGB values to CIEXYZ values, then CIELAB values and color differences are obtained in Section 2.2.

3 | THE PROPOSED METHOD

The schematic of our proposed method is shown in Figure 2. In our method, by analyzing the relationship among the standard color space (CIERGB, CIEXYZ, and CIELAB), we first construct the mapping relationship from the device RGB space to CIELAB color space based on backward-deduction method in Section 3.1. And then, in order to further improve the transformation accuracy, the high order extension polynomial method is introduced in Section 3.2.

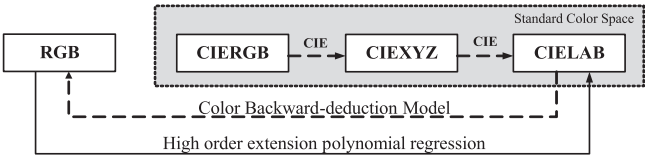

FIGURE 2 Schematic of our proposed method

3.1 | Mapping relationship between device RGB space and CIELAB space

It is generally known that the color difference in CIELAB space is used to evaluate the accuracy of color characterization method. So we need to map digital RGB values to CIELAB values through a series of transformations. It is easy to establish a relationship between CIERGB and CIEXYZ because of the linear transformation as shown in Equation (3). However, the relationship between CIEXYZ and CIELAB is nonlinear, which involves a cubic relevance. According to the standardized formula among CIE standard color values given in Section 2.2, Equation (5) can be transformed into multi-dimensional form

$$[L,a,b]^T = \boldsymbol{N} \times \left[f\left(\frac{X}{X_n}\right),f\left(\frac{Y}{Y_n}\right),f\left(\frac{Z}{Z_n}\right)\right]^T + \boldsymbol{V}, \quad (8)$$

where

$$\boldsymbol{N} = \begin{bmatrix} 0 & 116 & 0 \\ 500 & -500 & 0 \\ 0 & 200 & -200 \end{bmatrix} \text{ and } \boldsymbol{V} = [-16\ 0\ 0]^T. \quad (9)$$

Because of Equation (3), we have

$$\begin{bmatrix} X \\ Y \\ Z \end{bmatrix} = \begin{bmatrix} 2.7689 & 1.7517 & 1.1302 \\ 1.0000 & 4.5907 & 0.0601 \\ 0.0000 & 0.0565 & 5.5943 \end{bmatrix} \begin{bmatrix} R \\ G \\ B \end{bmatrix}$$

$$\Leftrightarrow \begin{bmatrix} \frac{X}{X_n} \\ \frac{Y}{Y_n} \\ \frac{Z}{Z_n} \end{bmatrix} = \begin{bmatrix} \frac{2.7689}{X_n} & \frac{1.7517}{X_n} & \frac{1.1302}{X_n} \\ \frac{1.0000}{Y_n} & \frac{4.5907}{Y_n} & \frac{0.0601}{Y_n} \\ 0.0000 & \frac{0.0565}{Z_n} & \frac{5.5943}{Z_n} \end{bmatrix} \begin{bmatrix} R \\ G \\ B \end{bmatrix}. \quad (10)$$

Furthermore, we have

$$\begin{cases} f\left(\frac{X}{X_n}\right) = \left(\frac{X}{X_n}\right)^{\frac{1}{3}} = \left(\frac{2.7689}{X_n}R + \frac{1.7517}{X_n}G + \frac{1.1302}{X_n}B\right)^{\frac{1}{3}} \\ f\left(\frac{Y}{Y_n}\right) = \left(\frac{Y}{Y_n}\right)^{\frac{1}{3}} = \left(\frac{1.0000}{Y_n}R + \frac{4.5907}{Y_n}G + \frac{0.0601}{Y_n}B\right)^{\frac{1}{3}}. \\ f\left(\frac{Z}{Z_n}\right) = \left(\frac{Z}{Z_n}\right)^{\frac{1}{3}} = \left(\frac{0.0000}{Z_n}R + \frac{0.0565}{Z_n}G + \frac{5.5943}{Z_n}B\right)^{\frac{1}{3}} \end{cases} \quad (11)$$

Then, we assume there exits the new vector $\left[(r^*)^{\frac{1}{3}}, (g^*)^{\frac{1}{3}}, (b^*)^{\frac{1}{3}}\right]^T$, which satisfies

$$\begin{bmatrix} f\left(\frac{X}{X_n}\right) \\ f\left(\frac{Y}{Y_n}\right) \\ f\left(\frac{Z}{Z_n}\right) \end{bmatrix} = \begin{bmatrix} \left(\frac{2.7689}{X_n}\right)^{\frac{1}{3}} & \left(\frac{1.7517}{X_n}\right)^{\frac{1}{3}} & \left(\frac{1.1302}{X_n}\right)^{\frac{1}{3}} \\ \left(\frac{1.0000}{Y_n}\right)^{\frac{1}{3}} & \left(\frac{4.5907}{Y_n}\right)^{\frac{1}{3}} & \left(\frac{0.0601}{Y_n}\right)^{\frac{1}{3}} \\ 0.0000 & \left(\frac{0.0565}{Z_n}\right)^{\frac{1}{3}} & \left(\frac{5.5943}{Z_n}\right)^{\frac{1}{3}} \end{bmatrix} \begin{bmatrix} (r^*)^{\frac{1}{3}} \\ (g^*)^{\frac{1}{3}} \\ (b^*)^{\frac{1}{3}} \end{bmatrix}. \quad (12)$$

Here a color characterization transformation is assumed as

$$\left[(r^*)^{\frac{1}{3}}, (g^*)^{\frac{1}{3}}, (b^*)^{\frac{1}{3}}\right]^T = \hat{\boldsymbol{M}} \cdot \hat{\boldsymbol{\rho}}\left(R^{\frac{1}{3}}, G^{\frac{1}{3}}, B^{\frac{1}{3}}\right), \quad (13)$$

where $\hat{\boldsymbol{M}}$ is the mapping matrix that depends Equations (11) and (12) and $\hat{\boldsymbol{\rho}}$ is a polynomial regression. Since digital RGB values are transformed to CIERGB values by polynomial regression and the matrix $\breve{\boldsymbol{M}}$, we can get

$$\hat{\rho}\left(R^{\frac{1}{3}}, G^{\frac{1}{3}}, B^{\frac{1}{3}}\right) = \breve{\boldsymbol{M}} \cdot \boldsymbol{\rho}\left(r^{\frac{1}{3}}, g^{\frac{1}{3}}, b^{\frac{1}{3}}\right). \quad (14)$$

The key to color characterization is to find the optimal mapping matrix $\boldsymbol{M} = \hat{\boldsymbol{M}} \cdot \breve{\boldsymbol{M}}$. By assuming

$$\boldsymbol{A}^* = \begin{bmatrix} \left(\frac{2.7689}{X_n}\right)^{\frac{1}{3}} & \left(\frac{1.7517}{X_n}\right)^{\frac{1}{3}} & \left(\frac{1.1302}{X_n}\right)^{\frac{1}{3}} \\ \left(\frac{1.0000}{Y_n}\right)^{\frac{1}{3}} & \left(\frac{4.5907}{Y_n}\right)^{\frac{1}{3}} & \left(\frac{0.0601}{Y_n}\right)^{\frac{1}{3}} \\ 0.0000 & \left(\frac{0.0565}{Z_n}\right)^{\frac{1}{3}} & \left(\frac{5.5943}{Z_n}\right)^{\frac{1}{3}} \end{bmatrix} \quad (15)$$

and letting $\boldsymbol{S}$ be a $m \times n$ matrix of vectors $[L, a, b]^T$, we can rewrite Equation (8) as follows:

$$\boldsymbol{S} = \boldsymbol{N} \cdot \boldsymbol{A}^* \cdot \boldsymbol{M} \cdot \boldsymbol{P} + \boldsymbol{V}. \quad (16)$$

By using the least square method, the transformation matrix can be derived as

$$\boldsymbol{M} = (\boldsymbol{A}^*)^{-1} \cdot \boldsymbol{N}^{-1} \cdot (\boldsymbol{S} - \boldsymbol{V}) \cdot \boldsymbol{P}^T / \left(\boldsymbol{P} \cdot \boldsymbol{P}^T\right). \quad (17)$$

Remark 3.1 A^* is derived from the simplification of Equation (11) to reduce computational complexity. Our future research will seek for a new A^* to make it closer to Equation (11) and will further improve the integrity of the model under this framework.

3.2 | Polynomial terms extension

In Section 3.1, we have established a better transformation from the device RGB space to CIELAB color space. To further improve the transformation accuracy, we propose polynomial terms extension in this section. The RPCC[19] is taking kth root of each k-order. Instead, our method adds the root polynomial terms to the k-order ordinary polynomial and ensures the order of each root polynomial term is equal to k. The polynomial expansions $\boldsymbol{\rho}_1^{14}, \boldsymbol{\rho}_2^{23}, \boldsymbol{\rho}_3^{42}, \boldsymbol{\rho}_4^{57}$ are denoted as follows:

$$
\begin{cases}
\rho_1^{14} = \left(1, r^{\frac{1}{3}}, g^{\frac{1}{3}}, b^{\frac{1}{3}}, \sqrt{r^{\frac{1}{3}}g^{\frac{1}{3}}}, \sqrt{g^{\frac{1}{3}}b^{\frac{1}{3}}}, \sqrt{r^{\frac{1}{3}}b^{\frac{1}{3}}}, \sqrt[3]{r^{\frac{1}{3}}g^{\frac{1}{3}}b^{\frac{1}{3}}}, \sqrt[3]{r^{\frac{1}{3}}g^{\frac{2}{3}}}, \sqrt[3]{r^{\frac{2}{3}}g^{\frac{1}{3}}}, \sqrt[3]{g^{\frac{1}{3}}b^{\frac{2}{3}}}, \sqrt[3]{g^{\frac{2}{3}}b^{\frac{1}{3}}}, \sqrt[3]{r^{\frac{1}{3}}b^{\frac{2}{3}}}, \sqrt[3]{r^{\frac{2}{3}}b^{\frac{1}{3}}}\right)^T \\
\rho_2^{23} = (1, r^{\frac{1}{3}}, g^{\frac{1}{3}}, b^{\frac{1}{3}}, \sqrt{r^{\frac{1}{3}}g^{\frac{1}{3}}}, \sqrt{g^{\frac{1}{3}}b^{\frac{1}{3}}}, \sqrt{r^{\frac{1}{3}}b^{\frac{1}{3}}}, \sqrt[3]{r^{\frac{1}{3}}g^{\frac{1}{3}}b^{\frac{1}{3}}}, \sqrt[3]{r^{\frac{1}{3}}g^{\frac{2}{3}}}, \sqrt[3]{r^{\frac{2}{3}}g^{\frac{1}{3}}}, \sqrt[3]{g^{\frac{1}{3}}b^{\frac{2}{3}}}, \sqrt[3]{g^{\frac{2}{3}}b^{\frac{1}{3}}}, \sqrt[3]{r^{\frac{1}{3}}b^{\frac{2}{3}}}, \sqrt[3]{r^{\frac{2}{3}}b^{\frac{1}{3}}}, \\
r^{\frac{2}{3}}, g^{\frac{2}{3}}, b^{\frac{2}{3}}, r^{\frac{1}{3}}g^{\frac{1}{3}}, r^{\frac{1}{3}}b^{\frac{1}{3}}, g^{\frac{1}{3}}b^{\frac{1}{3}}, \sqrt{r^{\frac{2}{3}}g^{\frac{1}{3}}b^{\frac{1}{3}}}, \sqrt{r^{\frac{1}{3}}g^{\frac{2}{3}}b^{\frac{1}{3}}}, \sqrt{r^{\frac{1}{3}}g^{\frac{1}{3}}b^{\frac{2}{3}}})T \\
\rho_3^{42} = (1, r^{\frac{1}{3}}, g^{\frac{1}{3}}, b^{\frac{1}{3}}, \sqrt{r^{\frac{1}{3}}g^{\frac{1}{3}}}, \sqrt{g^{\frac{1}{3}}b^{\frac{1}{3}}}, \sqrt{r^{\frac{1}{3}}b^{\frac{1}{3}}}, \sqrt[3]{r^{\frac{1}{3}}g^{\frac{1}{3}}b^{\frac{1}{3}}}, \sqrt[3]{r^{\frac{1}{3}}g^{\frac{2}{3}}}, \sqrt[3]{r^{\frac{2}{3}}g^{\frac{1}{3}}}, \sqrt[3]{g^{\frac{1}{3}}b^{\frac{2}{3}}}, \sqrt[3]{g^{\frac{2}{3}}b^{\frac{1}{3}}}, \sqrt[3]{r^{\frac{1}{3}}b^{\frac{2}{3}}}, \sqrt[3]{r^{\frac{2}{3}}b^{\frac{1}{3}}}, \\
r^{\frac{2}{3}}, g^{\frac{2}{3}}, b^{\frac{2}{3}}, r^{\frac{1}{3}}g^{\frac{1}{3}}, r^{\frac{1}{3}}b^{\frac{1}{3}}, g^{\frac{1}{3}}b^{\frac{1}{3}}, \sqrt{r^{\frac{2}{3}}g^{\frac{1}{3}}b^{\frac{1}{3}}}, \sqrt{r^{\frac{1}{3}}g^{\frac{2}{3}}b^{\frac{1}{3}}}, \sqrt{r^{\frac{1}{3}}g^{\frac{1}{3}}b^{\frac{2}{3}}}, \\
r, g, b, r^{\frac{1}{3}}g^{\frac{2}{3}}, r^{\frac{2}{3}}g^{\frac{1}{3}}, g^{\frac{1}{3}}b^{\frac{2}{3}}, g^{\frac{2}{3}}b^{\frac{1}{3}}, r^{\frac{1}{3}}b^{\frac{2}{3}}, r^{\frac{2}{3}}b^{\frac{1}{3}}, r^{\frac{1}{3}}g^{\frac{1}{3}}b^{\frac{1}{3}}, b^{\frac{2}{3}}\sqrt{r^{\frac{1}{3}}g^{\frac{1}{3}}}, r^{\frac{2}{3}}\sqrt{g^{\frac{1}{3}}b^{\frac{1}{3}}}, g^{\frac{2}{3}}\sqrt{r^{\frac{1}{3}}b^{\frac{1}{3}}}, r^{\frac{1}{3}}b^{\frac{1}{3}}\sqrt{r^{\frac{1}{3}}g^{\frac{1}{3}}}, \\
g^{\frac{1}{3}}b^{\frac{1}{3}}\sqrt{r^{\frac{1}{3}}g^{\frac{1}{3}}}, r^{\frac{1}{3}}g^{\frac{1}{3}}\sqrt{g^{\frac{1}{3}}b^{\frac{1}{3}}}, r^{\frac{1}{3}}b^{\frac{1}{3}}\sqrt{g^{\frac{1}{3}}b^{\frac{1}{3}}}, r^{\frac{1}{3}}g^{\frac{1}{3}}\sqrt{r^{\frac{1}{3}}b^{\frac{1}{3}}}, g^{\frac{1}{3}}b^{\frac{1}{3}}\sqrt{r^{\frac{1}{3}}b^{\frac{1}{3}}})T \\
\rho_4^{57} = (1, r^{\frac{1}{3}}, g^{\frac{1}{3}}, b^{\frac{1}{3}}, \sqrt{r^{\frac{1}{3}}g^{\frac{1}{3}}}, \sqrt{g^{\frac{1}{3}}b^{\frac{1}{3}}}, \sqrt{r^{\frac{1}{3}}b^{\frac{1}{3}}}, \sqrt[3]{r^{\frac{1}{3}}g^{\frac{1}{3}}b^{\frac{1}{3}}}, \sqrt[3]{r^{\frac{1}{3}}g^{\frac{2}{3}}}, \sqrt[3]{r^{\frac{2}{3}}g^{\frac{1}{3}}}, \sqrt[3]{g^{\frac{1}{3}}b^{\frac{2}{3}}}, \sqrt[3]{g^{\frac{2}{3}}b^{\frac{1}{3}}}, \sqrt[3]{r^{\frac{1}{3}}b^{\frac{2}{3}}}, \sqrt[3]{r^{\frac{2}{3}}b^{\frac{1}{3}}}, \\
r^{\frac{2}{3}}, g^{\frac{2}{3}}, b^{\frac{2}{3}}, r^{\frac{1}{3}}g^{\frac{1}{3}}, r^{\frac{1}{3}}b^{\frac{1}{3}}, g^{\frac{1}{3}}b^{\frac{1}{3}}, \sqrt{r^{\frac{2}{3}}g^{\frac{1}{3}}b^{\frac{1}{3}}}, \sqrt{r^{\frac{1}{3}}g^{\frac{2}{3}}b^{\frac{1}{3}}}, \sqrt{r^{\frac{1}{3}}g^{\frac{1}{3}}b^{\frac{2}{3}}}, \\
r, g, b, r^{\frac{1}{3}}g^{\frac{2}{3}}, r^{\frac{2}{3}}g^{\frac{1}{3}}, g^{\frac{1}{3}}b^{\frac{2}{3}}, g^{\frac{2}{3}}b^{\frac{1}{3}}, r^{\frac{1}{3}}b^{\frac{2}{3}}, r^{\frac{2}{3}}b^{\frac{1}{3}}, r^{\frac{1}{3}}g^{\frac{1}{3}}b^{\frac{1}{3}}, b^{\frac{2}{3}}\sqrt{r^{\frac{1}{3}}g^{\frac{1}{3}}}, r^{\frac{2}{3}}\sqrt{g^{\frac{1}{3}}b^{\frac{1}{3}}}, g^{\frac{2}{3}}\sqrt{r^{\frac{1}{3}}b^{\frac{1}{3}}}, r^{\frac{1}{3}}b^{\frac{1}{3}}\sqrt{r^{\frac{1}{3}}g^{\frac{1}{3}}}, \\
g^{\frac{1}{3}}b^{\frac{1}{3}}\sqrt{r^{\frac{1}{3}}g^{\frac{1}{3}}}, r^{\frac{1}{3}}g^{\frac{1}{3}}\sqrt{g^{\frac{1}{3}}b^{\frac{1}{3}}}, r^{\frac{1}{3}}b^{\frac{1}{3}}\sqrt{g^{\frac{1}{3}}b^{\frac{1}{3}}}, r^{\frac{1}{3}}g^{\frac{1}{3}}\sqrt{r^{\frac{1}{3}}b^{\frac{1}{3}}}, g^{\frac{1}{3}}b^{\frac{1}{3}}\sqrt{r^{\frac{1}{3}}b^{\frac{1}{3}}}, \\
r^{\frac{4}{3}}, g^{\frac{4}{3}}, b^{\frac{4}{3}}, rg^{\frac{1}{3}}, rb^{\frac{1}{3}}, gr^{\frac{1}{3}}, gb^{\frac{1}{3}}, br^{\frac{1}{3}}, bg^{\frac{1}{3}}, r^{\frac{2}{3}}g^{\frac{2}{3}}, g^{\frac{2}{3}}b^{\frac{2}{3}}, r^{\frac{2}{3}}b^{\frac{2}{3}}, r^{\frac{2}{3}}g^{\frac{1}{3}}b^{\frac{1}{3}}, g^{\frac{2}{3}}r^{\frac{1}{3}}b^{\frac{1}{3}}, b^{\frac{2}{3}}r^{\frac{1}{3}}g^{\frac{1}{3}})
\end{cases}
\tag{18}
$$

We increase the dimension of the base vector to improve the accuracy of the polynomial regression. Hong et al[12,13] pointed out that the regression accuracy in fact relies on the specific polynomial terms. Based on their research, only the 3-component cross term of $r^{\frac{1}{3}}$, $g^{\frac{1}{3}}$, $b^{\frac{1}{3}}$ are used for the polynomial expansions of quadratic and cubic polynomial. It is worth pointing out that the reduction of both the average ΔE and maximum ΔE is significantly subject to the three-dimensional cross term of $r^{\frac{1}{3}}$, $g^{\frac{1}{3}}$, $b^{\frac{1}{3}}$. For higher order polynomials, only the ordinary items are considered rather than root items because of the oscillating appearance. Compared with the methods mentioned in Section 2.3, our method increases the number of polynomial terms to improve the accuracy of color characterization. But for each $\rho_i^{[rgb]0.5,0.0,0.5n}(i=1,2,3,4)$, the highest degree of polynomial basis is $\frac{i}{3}$. The comparative tests will be performed in Section 4, which are based on such a standard selected basis. Although the number of base terms is different for these methods (mentioned in Section 2.3), this standard ensures that the comparison is reasonable and significant.

4 | EXPERIMENT

To verify the performance of our method, we test our method with the public data and carry out camera experiments. For each set of data, we compare the results with other methods mentioned in Section 2.3. The parameters for evaluating the performance of the method are include the mean ΔE_{ab} color difference (Section 2.2) for all color samples $\bar{\Delta E}$, the maximum ΔE_{ab} color difference ΔE_{max}, the mean error of each color attribute $\bar{\Delta L}$, $\bar{\Delta a}$, $\bar{\Delta b}$, the maximum error of each color attribute ΔL_{max}, Δa_{max}, Δb_{max}. In addition, ΔE, the error and the corrected error are all referring to the color difference in CIELAB color space without specification in this article.

4.1 | Tests with public data

We test our method using the numerical data given in the appendix of the literature[14] proposed by Hardeberg. The data is obtained from the AGFA Arcus II scanner with the AGFA IT8.7/2 color chart. Besides the characterization methods listed in the literature, we compare our method with the others.

Table 1 shows that our method obtains good results for each order polynomial, especially for the low-order-polynomial. When the first order polynomial of our method is used, the average ΔE is 1.013, which is much better compared by using Hardeberg's method. Meanwhile, both the average ΔE and the max ΔE have come close to the optimal results (ie, the results of the third

TABLE 1 Test results with public data

Model type	$\Delta\bar{E}$	ΔE_{max}	$\Delta\bar{L}$	ΔL_{max}	$\Delta\bar{a}$	Δa_{max}	$\Delta\bar{b}$	Δb_{max}
RGB–CIEXYZ,[12] $\boldsymbol{\rho}_1^4$	4.841	22.939	1.276	3.715	2.782	20.932	3.135	15.354
RGB–CIELAB,[20] $\boldsymbol{\rho}_1^4$	22.270	49.111	15.310	34.052	8.422	37.251	9.056	40.062
Hardeberg,[14] $\boldsymbol{\rho}_1^4$	5.652	23.961	3.241	11.345	2.234	23.304	2.987	12.645
RPCC,[19] $\boldsymbol{\rho}_1^3$	4.591	30.912	0.873	7.089	3.057	26.331	2.640	15.491
Our method, $\boldsymbol{\rho}_1^{14}$	1.013	4.782	0.342	2.547	0.569	3.313	0.591	3.389
RGB–CIEXYZ,[12] $\boldsymbol{\rho}_2^{10}$	2.989	28.246	0.458	3.585	1.653	21.718	1.956	28.089
RGB–CIELAB,[20] $\boldsymbol{\rho}_2^{10}$	8.858	40.349	2.854	14.054	5.077	25.858	5.024	29.930
Hardeberg,[14] $\boldsymbol{\rho}_2^{10}$	1.496	12.448	0.348	2.352	1.166	12.348	0.579	3.311
RPCC,[19] $\boldsymbol{\rho}_2^6$	4.530	22.746	0.707	2.743	2.830	20.962	2.899	13.362
Our method, $\boldsymbol{\rho}_2^{23}$	0.816	3.849	0.284	2.034	0.464	2.862	0.458	2.718
RGB–CIEXYZ,[12] $\boldsymbol{\rho}_3^{20}$	2.170	20.903	0.427	2.490	1.306	18.576	1.348	13.276
RGB–CIELAB,[20] $\boldsymbol{\rho}_3^{20}$	5.386	30.792	1.385	9.775	3.207	23.060	3.114	19.784
Hardeberg,[14] $\boldsymbol{\rho}_3^{20}$	0.918	4.666	0.289	2.069	0.621	4.588	0.427	2.792
RPCC,[19] $\boldsymbol{\rho}_3^{13}$	4.514	21.058	0.714	3.066	2.824	20.587	2.957	16.292
Our method, $\boldsymbol{\rho}_3^{42}$	0.629	3.213	0.251	1.746	0.326	2.418	0.363	2.341
RGB–CIEXYZ,[12] $\boldsymbol{\rho}_4^{35}$	1.537	14.269	0.301	2.716	0.912	12.222	0.95	11.197
RGB–CIELAB,[20] $\boldsymbol{\rho}_4^{35}$	3.565	20.605	0.835	7.765	2.238	17.501	1.984	10.34
Hardeberg,[14] $\boldsymbol{\rho}_4^{35}$	0.7	2.863	0.27	1.883	0.391	2.58	0.375	1.72
RPCC,[19] $\boldsymbol{\rho}_4^{22}$	4.04	23.161	0.641	2.919	2.529	22.207	2.587	18.576
Our method, $\boldsymbol{\rho}_4^{57}$	0.514	2.861	0.232	1.599	0.268	2.304	0.268	1.508

order polynomial) of Hardeberg's method. When the second order polynomial of our method is used, the average ΔE and the max ΔE have already outperformed the optimal results of Hardeberg's method. As for the third order polynomial, the max ΔE of our method is 3.213, which closes to the very good quality based on the color difference evaluation criterion introduced in Section 2.2. As we pointed the description in Remark 3.1, our method would deteriorate to Hardeberg's method if we use the classic polynomial expansion $\boldsymbol{\rho}_k^n$ mentioned in Section 2.1. However, we add root polynomial cross-terms to each order of the model and the added cross-terms are different from the ordinary polynomial cross-terms in that they are smoother around the achromatic region. From the test results, it can obviously improve the accuracy of color characterization.

As for RPCC method, it is unfair to be compared here as the number of polynomial terms is significantly different. From ρ_1 to ρ_4, RPCC has 3, 6, 13, and 22 terms and our method has 14, 23, 42, and 57 terms, but that is because the purpose between RPCC and our method is different. RPCC focuses on achieving exposure invariance, but our method aims to improve the accuracy of color characterization under the same exposure condition. On one hand, our color backward deduction model converts color signal from digital RGB to CIELAB space instead of CIEXYZ space (since the Euclidean distance in CIELAB space corresponds quite well to perceptual color differences), which can reduce the visual error of color characterization. On the other hand, based on RPCC method, high order extension of the polynomial root terms is proposed to improve the conversion accuracy further. Meanwhile, the performance of our method with low-order polynomial is comparable to that of other methods with high-order polynomial, which could help to reduce the influence of Runge effect. Although our method increases the number of polynomial terms, the highest degree of polynomial basis is $\frac{i}{3}$ for each $\rho_i^n(i=1,2,3,4)$, our method is an extension of RPCC method.

Then, we present the error analysis of our method in Figure 3 with the numerical data given in the literature.[14] The subgraph above is a scatter diagram that describes the corrected error of three channels for each patch in the public data. It is not difficult to find that the error of the red channel is relatively stable for the transformation. The error of the blue channel is much unstable compared with other channels. The following two subgraphs show the expectation and the variance of the corrected errors of the three channels for all patches. We find that the

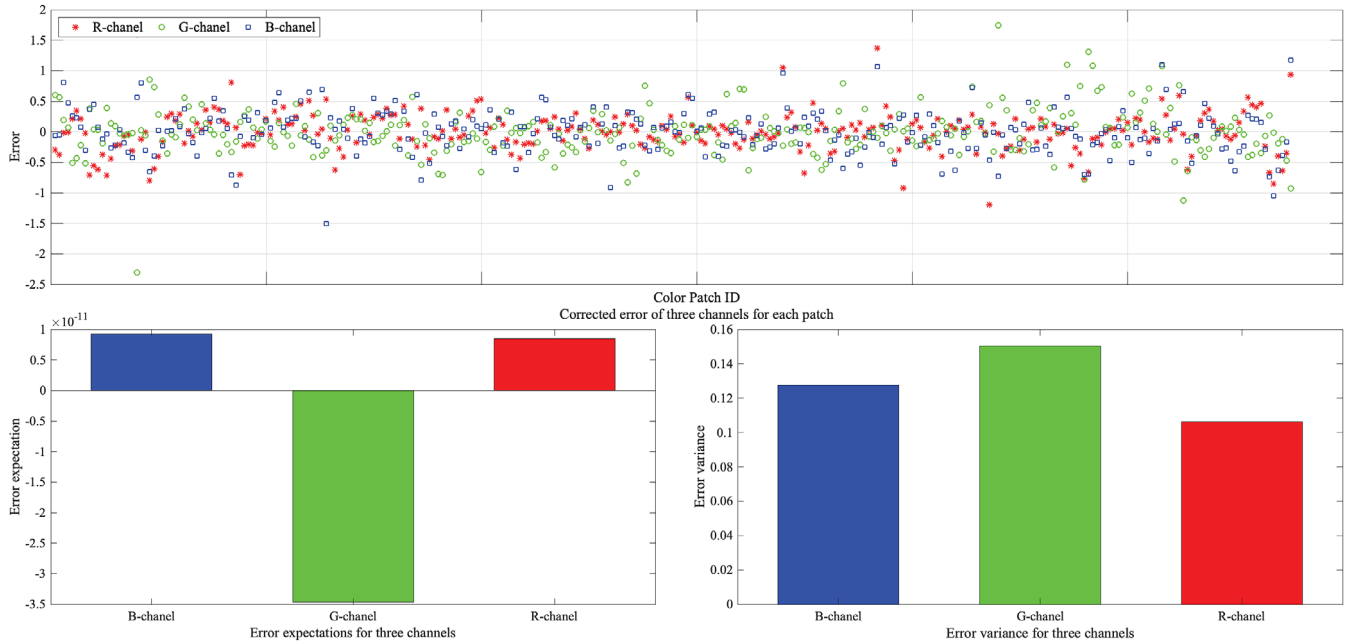

FIGURE 3 Error analysis of three channels with public data

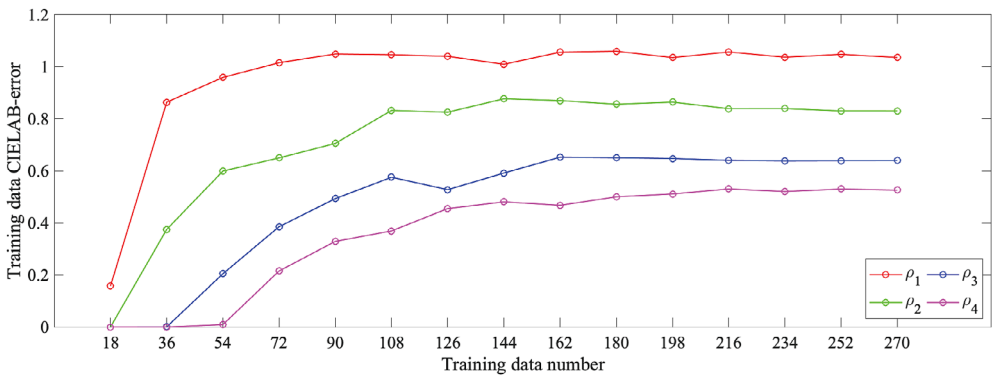

FIGURE 4 Corrected CIELAB error on the training set with public data

green channel is sensitive for transformation. The expected absolute value of the blue channel error is much higher.

To verify whether the results are overfit, we decrease the number of training data ($N_{training}$) used for regression. The other data ($N_{testing} = N - N_{training}$, $N = 288$) are used for testing. With our proposed method (from the first order to the fourth order polynomial), the corrected error on the training set and testing set are shown in Figures 4 and 5, respectively. As can be seen, when the number of training data is less than the number of parameters, the results are unstable. As the number of training data is increasing, the error converges to a constant value (from the first order to the fourth order polynomial) and the results become stable.

Furthermore, we compare the corrected error (ρ_4) with other methods (ρ_4) based on the testing data set. The results are shown in Table 2. It can be seen that even if the number of the training data is reduced to 108, the mean error of our method on the testing set only increases by 0.476 ΔE units. When the number of training data is larger than the number of parameters, the results of our method are obviously better than other three methods. Although the results get unusable with little sample, it is not a problem in practice since as much as possible data should be used for training to produce high quality results.

In the above experiments, the corrected errors are compared all in CIELAB color space. Since the classical methods convert the digital RGB to CIEXYZ color space, we also compare the corrected error of all the data (given

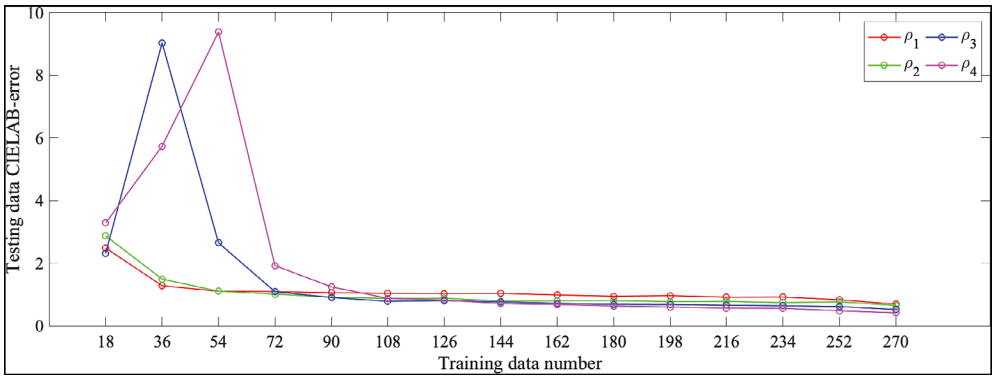

FIGURE 5 Corrected CIELAB error on the testing set with public data

TABLE 2 Corrected error on the testing set using the fourth order polynomial

Patches		Testing $\Delta\bar{E}$			
N_{traing}	$N_{testing}$	RGB–CIEXYZ,[12] ρ_4^{35}	RGB–CIELAB,[20] ρ_4^{35}	Hardeberg,[14] ρ_4^{35}	Our method, ρ_4^{57}
270	18	0.979	4.026	0.552	**0.435**
252	36	1.041	3.494	0.719	**0.517**
234	54	1.056	3.412	0.653	**0.514**
216	72	1.768	4.105	0.766	**0.616**
198	90	1.825	4.165	0.791	**0.638**
180	108	1.591	4.152	0.769	**0.646**
162	126	1.598	4.872	0.763	**0.701**
144	144	1.533	4.242	0.823	**0.754**
126	162	1.864	4.765	0.975	**0.822**
108	180	1.612	4.298	0.846	**0.911**
90	198	1.913	4.877	0.890	**1.155**
72	216	2.065	6.938	1.098	**2.810**
54	234	2.303	7.490	1.538	**12.561**
36	252	9.932	62.825	4.916	**6.328**

in the literature,[14] $N = 288$) in CIEXYZ color space with the classical methods. The comparison results are shown in Table 3. We also can see that even in CIEXYZ color space, the corrected error of our method is lower than that of the classical methods. The optimal result is obtained with the fourth order polynomial of our method.

The error analysis in CIEXYZ color space is similar to the overfitting experiment in CIELAB color space. We also gradually reduce the number of color patches used for training samples in the color checker, and the rest are test samples. The CIEXYZ error with our method based on the training set and testing set are shown in Figures 6 and 7, respectively. It can be seen that the CIEXYZ error trend of our method is similar to the CIELAB error trend above. The results are also stable and convergent.

TABLE 3 Corrected error of all data in CIEXYZ color space

Model type	$\bar{CIEXYZ}$ *error*
RGB–CIEXYZ,[12] ρ_1^4	1.141
RGB–CIELAB,[20] ρ_1^4	10.045
Our method, ρ_1^{14}	**0.559**
RGB–CIEXYZ,[12] ρ_2^{10}	0.721
RGB–CIELAB,[20] ρ_2^{10}	4.199
Our method, ρ_2^{23}	**0.459**
RGB–CIEXYZ,[12] ρ_3^{20}	0.511
RGB–CIELAB,[20] ρ_3^{20}	2.081
Our method, ρ_3^{42}	**0.386**
RGB–CIEXYZ,[12] ρ_4^{35}	0.396
RGB–CIELAB,[20] ρ_4^{35}	1.199
Our method, ρ_4^{57}	**0.332**

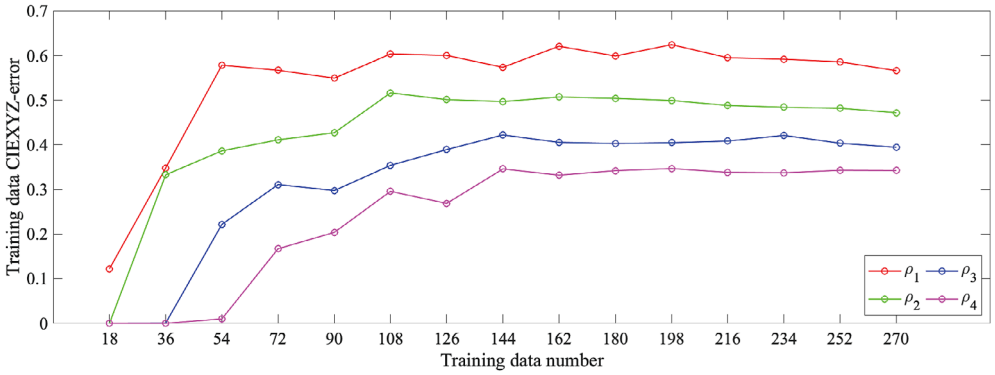

FIGURE 6 Corrected CIEXYZ error on the training set with public data

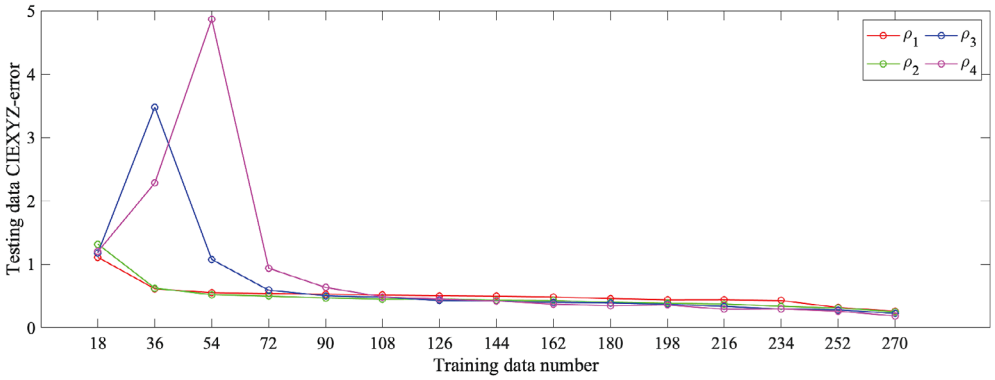

FIGURE 7 Corrected CIEXYZ error on the testing set with public data

In summary, based on the idea of RPCC method, our method expands terms to the basis of polynomial. Although the number of polynomial terms is increased, the result of color characterization is greatly improved and the computational complexity is not increased obviously. In addition, the first order polynomial results of our method are similar to the higher order polynomial results of other methods (eg, the results of Hardeberg's method (ρ_3^{20}) are similar to the results of our method (ρ_1^{14}), which means that our method could be helpful to reduce the influence of Runge effect and achieve exposure invariance with high conversion accuracy).

4.2 | Experiment with actual light source

We perform camera characterization under actual light source with the experimental set-up as shown in Figure 8. Two line illuminants project light on the surface of the object. The illuminants should be carefully set up in order to preserve the uniformity of light energy, which is crucial to the color characterization. A line scan camera is placed in the direction of the normal direction to the object surface while the lighting direction is projected at the angle of 45.

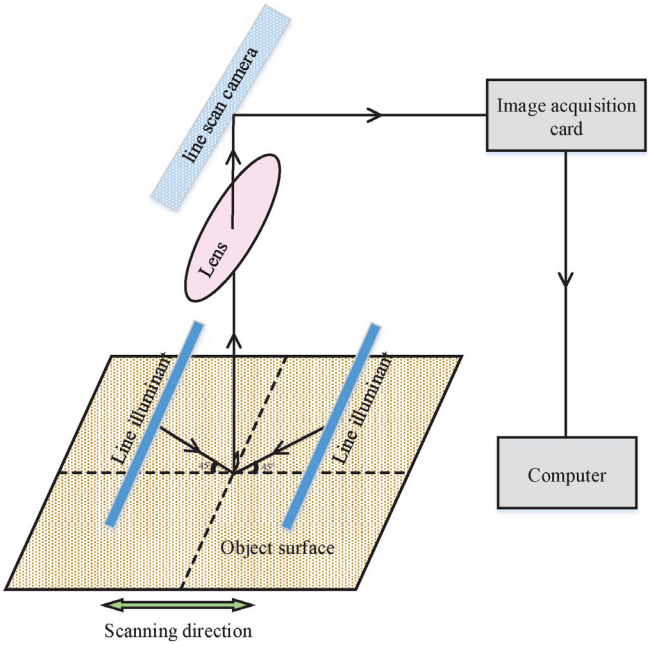

FIGURE 8 Schematic diagram of actual light source experimental set-up

TABLE 4 Experiment results with actual light source

Model type	$\bar{\Delta E}$	ΔE_{max}	$\bar{\Delta L}$	ΔL_{max}	$\bar{\Delta a}$	Δa_{max}	$\bar{\Delta b}$	Δb_{max}
RGB–CIEXYZ,[12] ρ_1^4	4.419	41.653	1.057	11.682	2.595	16.928	2.655	41.595
RGB–CIELAB,[20] ρ_1^4	13.955	43.347	5.672	23.717	7.259	27.000	7.936	33.710
Hardeberg,[14] ρ_1^4	5.379	48.766	1.351	12.460	3.235	47.764	3.173	27.281
RPCC,[19] ρ_1^3	4.419	41.653	1.057	11.682	2.595	16.927	2.655	41.595
Our method, ρ_1^{14}	**3.803**	**22.216**	**1.107**	**11.249**	**1.998**	**10.280**	**2.404**	**20.929**
RGB–CIEXYZ,[12] ρ_2^{10}	3.982	38.010	0.921	9.147	2.152	11.323	2.575	37.988
RGB–CIELAB,[20] ρ_2^{10}	7.366	23.650	2.577	17.009	3.801	18.563	4.497	21.125
Hardeberg,[14] ρ_2^{10}	4.262	21.941	0.986	10.436	2.334	21.502	2.774	20.131
RPCC,[19] ρ_2^6	4.438	37.732	1.251	14.177	2.362	11.724	2.774	37.178
Our method, ρ_2^{23}	**3.395**	**15.253**	**0.897**	**9.845**	**1.822**	**9.933**	**2.200**	**12.368**
RGB–CIEXYZ,[12] ρ_3^{20}	3.967	45.824	0.906	8.110	2.158	45.757	2.543	27.774
RGB–CIELAB,[20] ρ_3^{20}	4.858	16.812	1.393	13.148	2.658	13.459	3.031	15.231
Hardeberg,[14] ρ_3^{20}	3.555	13.064	0.884	9.904	1.845	10.688	2.348	10.876
RPCC,[19] ρ_3^{13}	4.238	34.136	1.201	13.425	2.138	10.574	2.782	32.665
Our method, ρ_3^{42}	**3.029**	**13.459**	**0.815**	**9.781**	**1.679**	**9.673**	**1.906**	**11.826**
RGB–CIEXYZ,[12] ρ_4^{35}	3.696	34.889	0.853	8.480	1.960	12.412	2.489	34.514
RGB–CIELAB,[20] ρ_4^{35}	3.758	14.323	0.953	11.589	2.132	11.008	2.288	11.238
Hardeberg,[14] ρ_4^{35}	3.177	13.318	0.817	9.698	1.723	9.643	2.036	10.807
RPCC,[19] ρ_4^{22}	4.054	40.682	1.083	12.673	2.143	11.070	2.634	39.472
Our method, ρ_4^{57}	**2.892**	**13.461**	**0.754**	**9.745**	**1.611**	**8.612**	**1.806**	**11.092**

When the equipment starts to work, the reflected light passes through the lens into the line scan camera, which can perform optical-electrical conversion. Finally, the image acquisition card captures the images and the computer saves the images. This equipment adopts line scan camera, which can capture only a line of the image at each time. Therefore, the imaging system is required to move along the main scanning direction until the collection of a frame image is finished.

The exposure should be set to prevent color clipping. Meanwhile, the aperture size and exposure time is fixed during the experiment. A X-Rite IT8.7/2 color chart on Kodak Ektacolour material is used. The color checker covers a large color gamut in CIELAB color space, whose nominal CIELAB values are specified by the manufacture. The raw images of the color checker are captured and the patches images are manually divided. Then we calculate the average responses of 90% of pixels in each patch, except for the marginalized pixels, as the output values of the camera RGB. The dark current is excluded from the average RGB responses. Next, the linearization of the camera RGB values is carried out to obtain RGB values proportional to the intensity of the input light. In addition, as the light source for this study is cultural relics-friendly linear array LED, the intensity distribution of this illuminant deceases generally from the middle to both sides, which results in high gray value in the middle of the captured image and low gray value in both sides. Therefore, a standard white board is used to correct the uniformity and repeatability of the captured image's brightness. Last, the linearized and homogenized camera RGB values and CIELAB- data are used to build the color characterization model described in Section 3. We test the model using the leave-one-out method. Specifically, the model is built based on all patches except one of the color checker. Then we test the model on the rest of the patches. The process is repeated for all patches and the mean ΔE in CIELAB color space is calculated. The results can be seen in Table 4.

From the table, we can see that our method performs better than other four methods and gives good results, that is, the mean ΔE is below three units when the fourth order polynomial is used. When comparing the results with the color difference rules mentioned in Section 2.2, the average error is hardly perceptible and the maximal error is acceptable. It is worth pointing out that the number of polynomial terms in our method has increased, which might seem unfair to other methods in a sense. However, the main purpose of our method is to pursue higher accuracy and better stability, which is mainly

Patches		Testing error		
Ntraing	Ntesting	Hardeberg,[14] ρ_5^{56}	Hardeberg,[14] ρ_4^{35}	Our method, ρ_4^{57}
198	90	5.042	4.483	4.192

TABLE 5 Corrected error on the testing set with actual light source experiment

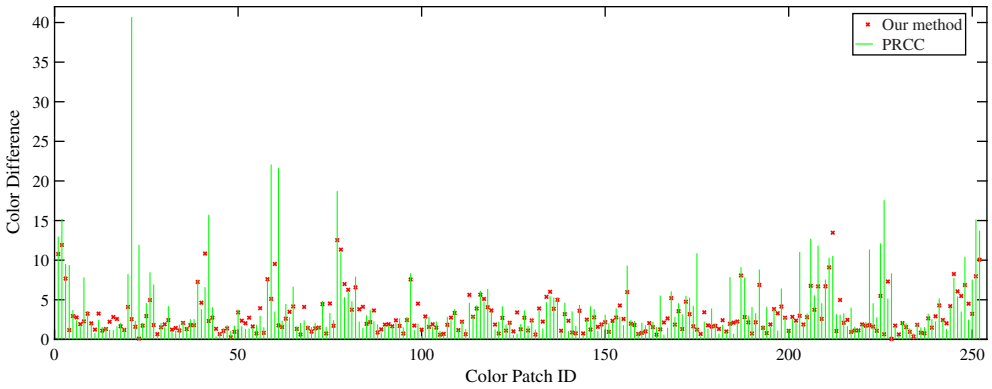

FIGURE 9 Color difference comparison between our method and RPCC using fourth order polynomial ($\rho 4$)

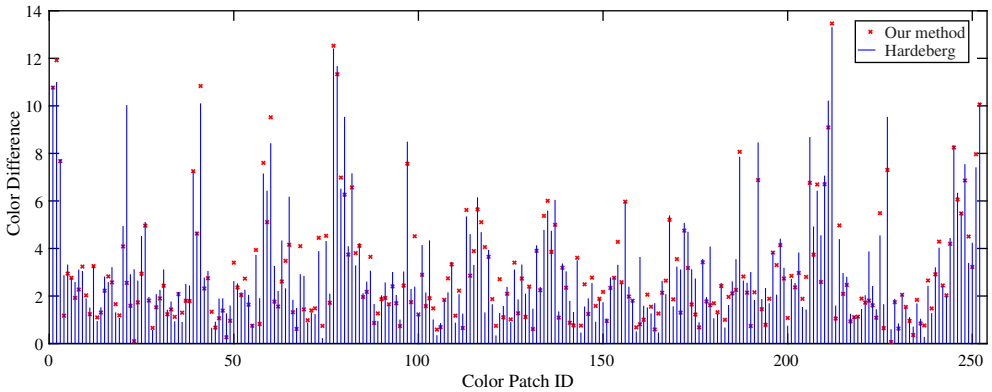

FIGURE 10 Color difference comparison between our method and Hardeberg's method using fourth order polynomial ($\rho 4$)

manifested in the following two aspects: First, the performance of our method with low-order polynomials is comparable to that of other methods with high-order polynomials, which could help to reduce the influence of Runge effect. Second, compared with other methods, the increased terms of our method were root polynomial cross-terms. Above all, cross-terms played an important role in improving prediction accuracy.[12] and then the root polynomial cross-terms are different from the ordinary polynomial cross-terms, in particular they are smoother around the achromatic region,[19] so the terms we have added could improve the results of color characterization.

In order to illustrate the impact of the Runge phenomenon, we choose the fourth order polynomial, because our focus is on higher color characterization accuracy. One hundred and ninety-eight color patches in the color checker are used as training samples, and the remaining 90 color patches are used as test samples. The error produced by Hardeberg's method and our method with test samples is shown in Table 5.

It can be seen from the table that our method is superior to Hardeberg's method with the fourth order polynomial. When the higher order polynomial is used, Hardeberg's method should produce a better result. However, due to the impact of Runge effect, the result gets worse. Therefore, our method is helpful to reduce the impact of Runge effect and obtain higher accuracy of color characterization.

The color difference comparisons between our method and each other method for each color patch are shown in Figures 9-12. It can be seen that the color corrected error of each patch in our method is significantly lower than that in other four methods. For some patches, such as the patches with low lightness, they have a relatively high color error due to low signal-to-noise

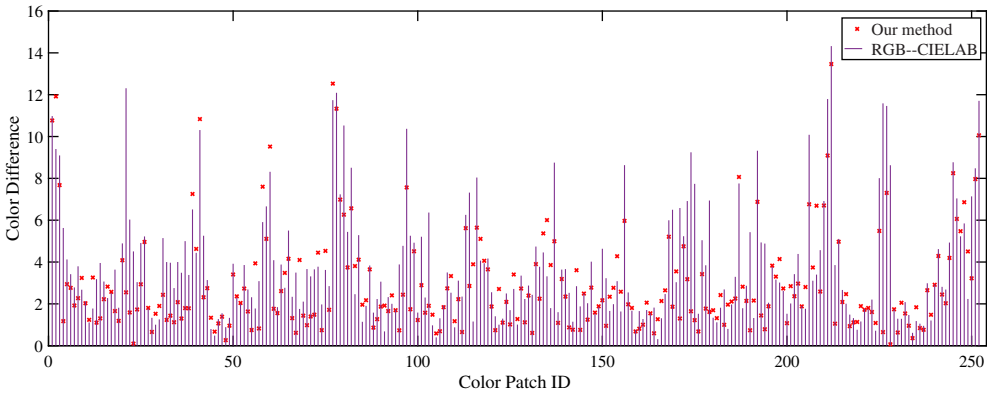

FIGURE 11 Color difference comparison between our method and RGB–CIELAB using fourth order polynomial ($\rho 4$)

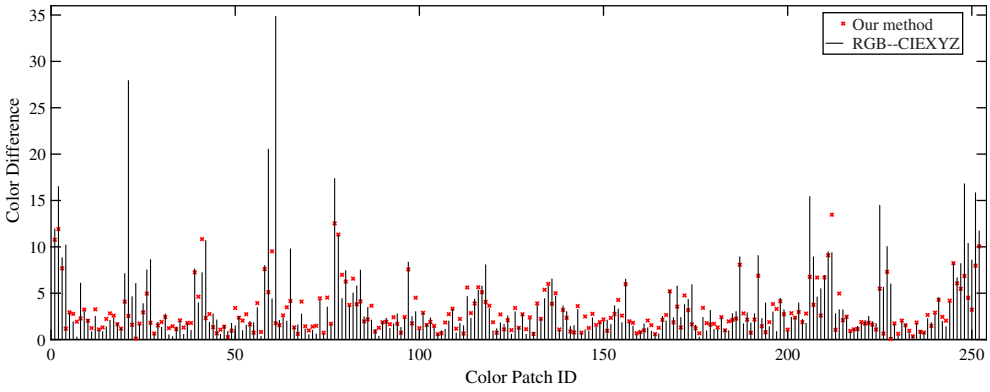

FIGURE 12 Color difference comparison between our method and RGB–CIEXYZ using fourth order polynomial ($\rho 4$)

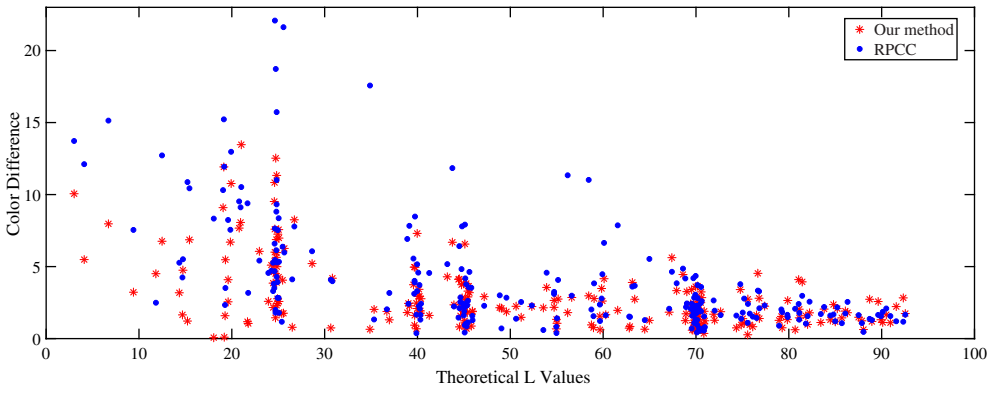

FIGURE 13 The plot of the relation between color corrected error and L color component using fourth order polynomial ($\rho 4$)

ratio of the camera, but our method is still superior to other four methods.

Furthermore, in order to analyze the relationship between color corrected errors and color attributes, ΔE vs L, ΔE vs a and ΔE vs b of our method and RPCC method with the fourth order polynomial are shown respectively in Figures 13-15. In Figure 13, we can see that color samples with high brightness are more accurate than the ones with low brightness. In Figures 14 and 15, the neutral colors have lower corrected accuracy. Dark neutral colors have the maximal color corrected errors. The results in Figures 13-15 suggest that our method has advantages in color characterization with lower brightness and neutral colors.

In order to illustrate whether the color characterization model can be normalized in practical application, we divide the color patches of the X-Rite IT8.7/2 color chart as described in Section 4.1 (systematically reduce the number of training samples, and the rest are test samples). The results with our method under the actual light source are reported in Figures 16 and 17. From the figures, the errors of the color characterization model are still convergent and stable in practice.

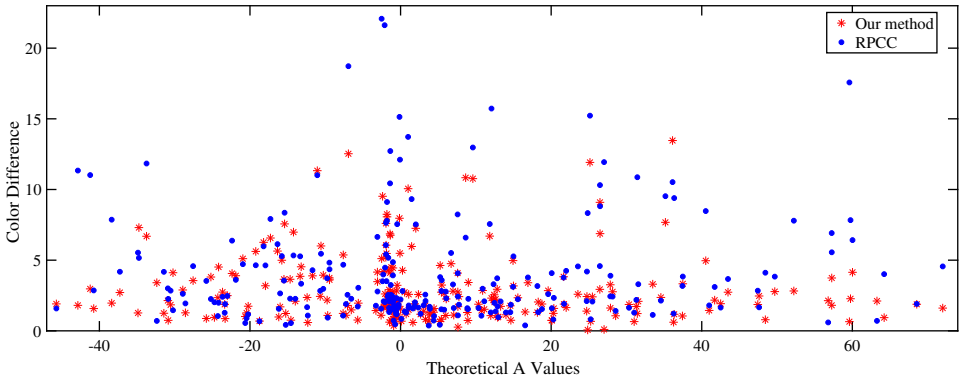

FIGURE 14 The plot of the relation between color corrected error and A color component using fourth order polynomial ($\rho 4$)

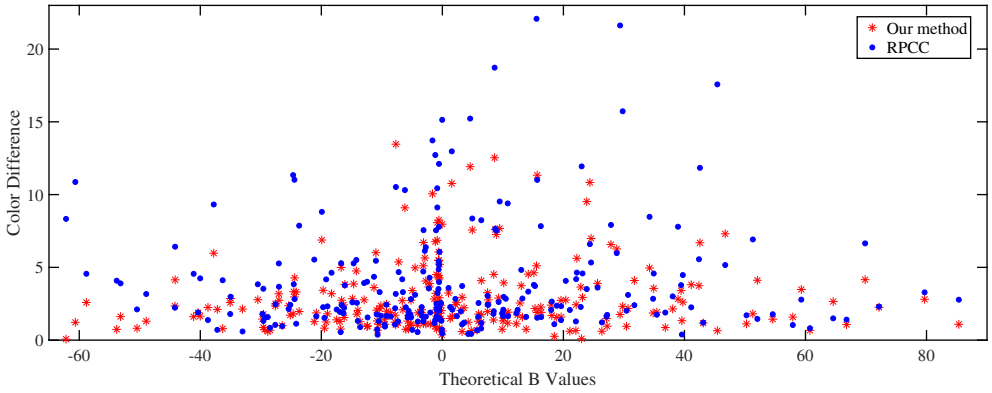

FIGURE 15 The plot of the relation between color corrected error and B color component using fourth order polynomial ($\rho 4$)

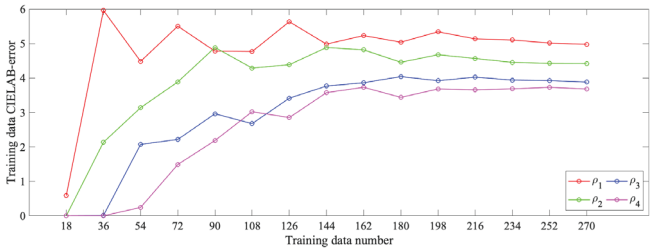

FIGURE 16 Corrected CIELAB error on the training set with actual light source

Furthermore, we use a new chart (Macbeth ColorChecker) as the test sample and the X-Rite IT8.7/2 color chart as the training sample for the test. The errors of the test sample are shown in Table 6. As can be seen from the results, our method works well.

Finally, to illustrate the noise influence on the color characterization model, we add 1%, 5%, and 10% gaussian noise to the X-Rite IT8.7/2 color chart and then compute the three noise color charts for color correction. The results are shown in Table 7. It can be seen that the noise leads the corrected error to be higher, but the errors can be controlled. The results become better as the degree of the polynomial increases. Compared with the color difference evaluation standard proposed in Section 2.2, the color correction effect is acceptable even with 10% gaussian noise.

4.3 | Statistical analysis

The statistical analysis method was used to check whether the improvement is significant or not between our method and other methods. As CIEDE2000 is more close to perceptual difference, *T*-test based on CIEDE2000 color differences was used for statistical analysis. According to the test results of public data (Table 1) and the experiment results with actual light source (Table 4), we compared and analyzed the CIEDE2000 color differences between our method and other methods for each order of the polynomial model. The results are shown in Tables 8 and 9.

It can be seen that *P* values are all less than .01 for each order polynomial, which implies that the reduction of the corrected error with our method reaches an extremely significant level.

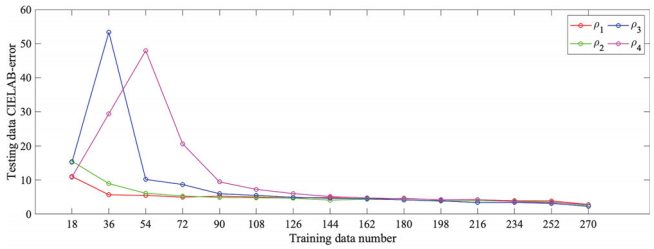

FIGURE 17 Corrected CIELAB error on the testing set with actual light source

5 | CONCLUSIONS

In this article, we propose a complete transformation model form digital RGB responses to CIELAB colorimetric values considering the interrelations among the standard CIE color spaces. Moreover, the polynomial root terms extension is constructed to improve further the transformation accuracy. The test data given in the literature are used to compare the proposed method and the previous methods. Besides, camera experiments are carried out to verify the performance of

TABLE 6 Corrected error of Macbeth ColorChecker

	RGB–CIEXYZ[12]	RGB–CIELAB[20]	RPCC[19]	Hardeberg[14]	Our method
	$\boldsymbol{\rho}_4^{35}$	$\boldsymbol{\rho}_4^{35}$	$\boldsymbol{\rho}_4^{22}$	$\boldsymbol{\rho}_4^{35}$	$\boldsymbol{\rho}_4^{57}$
$\Delta\bar{E}$	4.115	4.923	5.312	3.501	3.073

TABLE 7 Corrected error of noise color checkers

Model type	No noise, $\Delta\bar{E}$	1% noise, $\Delta\bar{E}$	5% noise, $\Delta\bar{E}$	10% noise, $\Delta\bar{E}$
Our method, $\boldsymbol{\rho}_1^{14}$	3.803	4.384	4.692	6.182
Our method, $\boldsymbol{\rho}_2^{23}$	3.395	3.919	4.274	5.541
Our method, $\boldsymbol{\rho}_3^{42}$	3.029	3.456	3.738	5.029
Our method, $\boldsymbol{\rho}_4^{57}$	2.892	3.276	3.668	4.819

TABLE 8 *T*-test results based on CIEDE2000 color difference with public data

Method	Mean difference	SD difference	*T*-value	*P*-value
Our method, $\rho_4^{57} \leftrightarrow$ Hardeberg,[14] ρ_4^{35}	−0.10257	0.18751	−9.283	.000
Our method, $\rho_4^{57} \leftrightarrow$ RGB-CIELAB,[20] ρ_4^{35}	−1.86463	1.64297	−19.260	.000
Our method, $\rho_4^{57} \leftrightarrow$ RGB-CIEXYZ,[12] ρ_4^{35}	−0.55128	0.97011	−9.644	.000
Our method, $\rho_4^{57} \leftrightarrow$ RPCC,[19] ρ_4^{22}	−2.1324	2.22509	−16.264	.000
Our method, $\rho_3^{42} \leftrightarrow$ Hardeberg,[14] ρ_3^{20}	−0.15643	0.28662	−9.262	.000
Our method, $\rho_3^{42} \leftrightarrow$ RGB-CIELAB,[20] ρ_3^{20}	−2.66797	2.09659	−21.595	.000
Our method, $\rho_3^{42} \leftrightarrow$ RGB-CIEXYZ,[12] ρ_3^{20}	−0.82158	1.29813	−10.741	.000
Our method, $\rho_3^{42} \leftrightarrow$ RPCC,[19] ρ_3^{13}	−2.35474	2.36113	−16.925	.000
Our method, $\rho_2^{23} \leftrightarrow$ Hardeberg,[14] ρ_2^{10}	−0.40703	0.61233	−11.281	.000
Our method, $\rho_2^{23} \leftrightarrow$ RGB-CIELAB,[20] ρ_2^{10}	−4.77969	2.84867	−28.474	.000
Our method, $\rho_2^{23} \leftrightarrow$ RGB-CIEXYZ,[12] ρ_2^{10}	−1.13161	1.53601	−12.503	.000
Our method, $\rho_2^{23} \leftrightarrow$ RPCC,[19] ρ_2^{56}	−2.11243	1.84665	−19.413	.000
Our method, $\rho_1^{14} \leftrightarrow$ Hardeberg,[14] ρ_1^{54}	−1.25276	1.51699	−14.015	.000
Our method, $\rho_1^{14} \leftrightarrow$ RGB-CIELAB,[20] ρ_1^{54}	−8.38228	3.57010	−39.845	.000
Our method, $\rho_1^{14} \leftrightarrow$ RGB-CIEXYZ,[12] ρ_1^{54}	−2.21035	2.29872	−17.346	.000
Our method, $\rho_1^{14} \leftrightarrow$ RPCC,[19] ρ_1^{53}	−2.00926	2.09754	−16.256	.000

TABLE 9 *T*-test results based on CIEDE2000 color difference with experiment

Method	Mean difference	SD difference	*T*-value	*P*-value
Our method, $\rho_4^{57} \leftrightarrow$ Hardeberg,[14] ρ_4^{35}	−0.15154	0.67813	−3.547	.000
Our method, $\rho_4^{57} \leftrightarrow$ RGB-CIELAB,[20] ρ_4^{35}	−0.51550	1.21774	−6.720	.000
Our method, $\rho_4^{57} \leftrightarrow$ RGB-CIEXYZ,[12] ρ_4^{35}	−0.41956	1.72089	−3.870	.000
Our method, $\rho_4^{57} \leftrightarrow$ RPCC,[19] ρ_4^{22}	−0.63230	1.80184	−5.571	.000
Our method, $\rho_3^{42} \leftrightarrow$ Hardeberg,[14] ρ_3^{20}	−0.30349	0.77720	−6.199	.000
Our method, $\rho_3^{42} \leftrightarrow$ RGB-CIELAB,[20] ρ_3^{20}	−1.02765	1.43540	−11.365	.000
Our method, $\rho_3^{42} \leftrightarrow$ RGB-CIEXYZ,[12] ρ_3^{20}	−0.45336	1.70700	−4.216	.000
Our method, $\rho_3^{42} \leftrightarrow$ RPCC,[19] ρ_3^{13}	−0.64253	1.68518	−6.053	.000
Our method, $\rho_2^{23} \leftrightarrow$ Hardeberg,[14] ρ_2^{10}	−0.48138	1.25277	−6.100	.000
Our method, $\rho_2^{23} \leftrightarrow$ RGB-CIELAB,[20] ρ_2^{10}	−2.40880	2.17190	−17.606	.000
Our method, $\rho_2^{23} \leftrightarrow$ RGB-CIEXYZ,[12] ρ_2^{10}	−0.27844	1.32070	−3.347	.001
Our method, $\rho_2^{23} \leftrightarrow$ RPCC,[19] ρ_2^{6}	−0.53408	1.56796	−5.407	.000
Our method, $\rho_1^{14} \leftrightarrow$ Hardeberg,[14] ρ_1^{4}	−0.99449	2.07450	−7.610	.000
Our method, $\rho_1^{14} \leftrightarrow$ RGB-CIELAB,[20] ρ_1^{4}	−5.50778	3.04385	−28.725	.000
Our method, $\rho_1^{14} \leftrightarrow$ RGB-CIEXYZ,[12] ρ_1^{4}	−0.25818	1.37484	−2.981	.003
Our method, $\rho_1^{14} \leftrightarrow$ RPCC,[19] ρ_1^{3}	−0.25818	1.37484	−2.981	.003

our method. The results show that the method presented in this article outperforms its predecessors in color characterization accuracy. Our method borrows from the idea of RPCC method, but it is different from RPCC. The main purpose is to improve the accuracy of color characterization under the same exposure condition. Moreover, the computational complexity does not increase significantly, so the proposed method is an extension of RPCC method. When new data is captured under different light sources, the color information is affected by the intensity of light sources, the color temperature of light sources, capture equipments and other factors, so it is necessary to recharacterization under the new light source. In addition, it should be note that some researchers used camera's RGB responses or tristimulus values for recovering the spectral information from the colorimetric information.[22-24] With the method proposed in this article, colorimetric error can be reduced significantly, therefore, the spectral reproduction results can be further improved.

ACKNOWLEDGMENT

This work is supported by National Natural Science Foundation of China (No. 11601416), the China Postdoctoral Science Foundation (No. 2018M640968), and the Fundamental Research Funds for the Central Universities (No. XTR042019005).

ORCID

Jing Ji https://orcid.org/0000-0002-7365-1125
Suping Fang https://orcid.org/0000-0002-3991-9650

REFERENCES

[1] Molada-Tebar A, Lerma Luis J, Marqués-Mateu A. Camera characterization for improving color archaeological documentation. *Color Res Appl*. 2017;43(14):47-57.
[2] Barni M, Pelagotti A, Piva A. Image processing for the analysis and conservation of paintings: opportunities and challenges. *Signal Process Mag IEEE*. 2005;22(5):141-144.
[3] Parry R. Digital heritage and the rise of theory in museum computing. *Museum Manage Curatorship*. 2005;20(4):333-348.
[4] Sharma G, Bala R. *Digital Color Imaging Handbook*. Boca Raton, FL: CRC Press; 2010.
[5] Hung PC. Colorimetric calibration for scanners and media. *Proc SPIE*. 1991;1448:164-174.
[6] Hung PC. Colorimetric calibration in electronic imaging devices using a look-up table model and interpolations. *Electron Imaging*. 1993;2:53-61.
[7] Kang HR. Colour scanner calibration. *Imaging Sci Technol*. 1992;36:162-170.
[8] Kang HR, Anderson PG. Neural network applications to the colour scanner and printer calibrations. *Electron Imaging*. 1992;1:125-134.
[9] Johnson T. Methods for characterizing colour scanners and digital cameras. *Displays*. 1996;16(4):183-191.
[10] Mou TS, Shen HL. Colorimetric characterization of imaging device by total color difference minimization. *J Zhejiang Univ Sci A Appl Phys Eng*. 2006;7(6):1041-1045.
[11] Kang HR, Anderson PG. Neural network applications to the color scanner and printer calibrations. *J Electron Imaging*. 1992;1(1):125-135.
[12] Hong G, Luo MR, Rhodes PA. A study of digital camera colorimetric characterization based on polynomial modeling. *Color Res Appl*. 2001;26(1):76-84.

[13] Hong G, Han B, Luo MR. Colorimetric characterisation of low-end digital camera and its application for on-screen texture visualisation. Paper presented at: International Conference on Image Processing IEEE; 2000.
[14] Hardeberg JY. *Acquisition and Reproduction of Colour Images: Colorimetric and Multispectral Approaches*. Parkland, FL: Universal Publishers Dissertation.com; 2001.
[15] Hardeberg JY, Schmitt F, Tastl I, Brettel H, Crettez JP. Color management for color facsimile. Paper presented at: Proc. IS&T and SID's 4th Color Imaging Conf.: Color Science, Systems and Applications, Scottsdale; 1996. pp. 108–113.
[16] Andersen CF, Hardeberg JY. Colorimetric characterization of digital cameras preserving hue planes. Paper presented at: Proc. 13th Color Imag. Conf. (CIC); 2005. pp. 141–146.
[17] Huang X, Yu H, Shi J, Tai Y. Improvement on the polynomial modeling of digital camera colorimetric characterization. *Optoelectronic Imaging and Multimedia Technology III*. Beijing, China: International Society for Optics and Photonics; 2014.
[18] Finlayson GD, Drew M. Constrained least-squares regression in color spaces. *Electron Imaging*. 1997;6(4):484-493.
[19] Finlayson GD, Mackiewicz M, Hurlbert A. Color correction using root-polynomial regression. *IEEE Trans Image Process*. 2015;24(5):1460-1470.
[20] Sun B, Liu H, Zhou S, Li W. Evaluating the performance of polynomial regression method with different parameters during color characterization. *Math Probl Eng*. 2014;2014(1):1-7.
[21] Abrardo A, Cappellini V, Cappellini M, Mecocci A. Art-works colour calibration using the VASARI scanner. Paper presented at: Proceedings of IS&T and SID's 4th Color Imaging Conference. Color Science, Systems and Applications; 1996. pp. 94–97.
[22] Zhang X, Wang Q, Li J, Zhou X, Yang Y, Xu H. Estimating spectral reflectance from camera responses based on CIE XYZ tristimulus values under multiilluminants. *Color Res Appl*. 2017;42(1):68-77.
[23] Cao B, Liao N, Cheng H. Spectral reflectance reconstruction from RGB images based on weighting smaller color difference group. *Color Res Appl*. 2017;42(3):327-332.
[24] Amiri MM, Fairchild MD. A strategy toward spectral and colorimetric color reproduction using ordinary digital cameras. *Color Res Appl*. 2018;43:675-684.

AUTHOR BIOGRAPHIES

Jing Ji received a BS degree in computer science and technology and an MS degree in computer application technology from Chang'an University, Xi'an, China, in 2005 and 2008, respectively. She is currently a doctoral student at the School of Mechanical Engineering, Xi'an Jiaotong University. Her research interests reside in colorimetry and digital image processing.

Suping Fang received BS and MS degrees from Xi'an Jiaotong University in 1983 and 1986, respectively. He received a PhD in precision engineering from Kyoto University, Japan, in 1996. From 1996 to 2004, he worked successively at Kyoto University, Ritsumeikan University in Japan. Currently, he is a Professor at Xi'an Jiaotong University. His research interests mainly focused on high fidelity digitization of cultural heritage involving colorimetry, digital image processing, and optical electromechanical integration technology.

Zhengyuan Shi received a BS degree from Nanjing Agricultural University, China in 2018. Now he is a graduate student in Xi'an Jiaotong University. His research interests include computational fluid dynamics, image processing, and scientific computing.

Qing Xia received a BS degree from Xi'an Jiaotong University, China in 2019. Now he is a graduate student in Xi'an Jiaotong University. His research interests include additive manufacturing (3D Printing), image processing, and scientific computing.

Yibao Li received the MS and PhD degrees in applied mathematics from Korea University, Seoul, Korea, in 2011 and 2013, respectively. Before he joined the School of Mathematics and Statistics, Xi'an Jiaotong University, China in 2014, he held a research position in Department of Computational Science and Engineering, Yonsei University, Seoul, Korea. He is currently an associate professor in the Department of Applied Mathematics. His research interests include image processing, computational fluid dynamics, and scientific computing.

How to cite this article: Ji J, Fang S, Shi Z, Xia Q, Li Y. An efficient nonlinear polynomial color characterization method based on interrelations of color spaces. *Color Res Appl*. 2020; 1–17. https://doi.org/10.1002/col.22563